Integrated Master in Chemical Engineering

Selective removal of CO_2 using kinetic UPRM-5 adsorbent

Master's Thesis

by

Ana Isabel Silva Leitão

SINTEF – Materials and Chemistry

FEUP Supervisor: **Prof. José Miguel Loureiro**

SINTEF Supervisor: **Dr. Carlos A. Grande**

Departamento de Engenharia Química

February 2016

Acknowledgments

I would like to express my sincere gratitude to my supervisors Dr. Carlos A. Grande at SINTEF and Professor José Miguel Loureiro at FEUP, for allowing me to take part in this exciting project abroad and providing guidance over this internship. During this time I was able to grow a lot academically and as a human being, thanks to them and to this whole experience.

I'm particularly grateful for the assistance given by Ann Lind at SINTEF with the XRD analysis and experimental data treatment.

I wish to acknowledge the great help of Giorgia Mondino during the gathering of the adsorption isotherms, as well as her advice related to the tricky Gas Chromatograph operation.

For the continuous support, motivation and friendship throughout the dissertation period, I would like to show my sincere gratitude to the people that play the most important role in my life: my tireless and caring boyfriend, my loving family as well as my good college friends.

The support of the Research Council of Norway through the CLIMIT program by the SINTERCAP project (233818). This publication has been produced with support from the BIGCCS Centre, performed under the Norwegian research program Centres of Environment-friendly Energy Research (FME). The author acknowledges the following partners for their contributions: ConocoPhillips, Gassco, Shell, Statoil, TOTAL, GDF SUEZ and the Research Council of Norway (193816/S60).

Abstract

Climate changes experience nowadays, enhanced the urgent need for a transition to less pollutant energy sources. Natural gas is the fossil fuel with lower carbon content making it the reasonable fuel of choice. In natural gas processing, CH_4/CO_2 separation is quite relevant. Adsorption is starting to be a more appealing technique to implement this separation, ever since adsorbents with flexible structures, were discovered. Sr^{2+}UPRM5 was studied to separate kinetically both components. The equilibrium and kinetic properties of the adsorbent were studied through adsorption equilibrium isotherms, and breakthrough curves. XRD analysis took place to determine the better temperature activation range.

Adsorption Isotherms of carbon dioxide and methane were measured at 25ºC and fitted to the Sips model. The adsorbent showed higher affinity towards CO_2.

Breakthrough experiments were performed using two different methods, the traditional breakthrough curves and temperature programmed desorption breakthrough curves. A mathematical model was used to simulate the breakthrough curves using the *gProms* software.

All the experiments were conclusive about the kinetic effects of adsorption of both components on the adsorbent.

Keywords: Natural Gas, Methane, Carbon Dioxide, Adsorption, Kinetics, PSA

Resumo

As atuais alterações climáticas, criaram a necessidade urgente de transição para fontes energéticas menos poluentes. O gás natural é o combustível fóssil com menor teor de carbono tornando-o o combustível de escolha mais razoável. No processamento de gás natural, a separação CH_4 / CO_2 é de importância relevante. A Adsorção tornou-se uma técnica ainda mais apelativa para processar essa separação, a partir do momento em que adsorventes com estruturas flexíveis foram descobertos.

Sr^{2+}UPRM-5 foi estudado para separar cineticamente ambos os componentes. Estudaram-se as propriedades de equilíbrio e cinéticas do adsorvente por meio de isotérmicas de equilíbrio de adsorção, e curvas de rutura. Fez-se uma análise XRD para determinar a melhor gama de ativação de temperatura.

As Isotérmicas de adsorção de dióxido de carbono e metano foram medidas a 25ºC e ajustadas ao modelo de Sips. O adsorvente apresentou maior afinidade para com o CO_2.

Foram realizadas experiências de curvas de rutura, utilizando dois métodos diferentes, tradicionais e de dessorção a temperatura programada. Um modelo matemático foi usado para simular as curvas de rutura utilizando o software gPROMS.

Todas as experiências foram conclusivas sobre os efeitos cinéticos na adsorção de ambos os componentes no adsorvente Sr^{2+}UPRM-5.

Official Statement

I declare, under honour commitment, that the present work is original and that every non original contribution was properly referred, by identifying its origins.

Ana Isabel Silva Leitão

Table of Contents

List of Figures

List of Tables

Glossary

C	bulk molar concentration of the component *i* in the gas phase	$mol.m^{-3}$
C_0	initial component *i* bulk molar concentration	$mol.m^{-3}$
C_p	component *i* bulk molar concentration in the adsorbents pores	$mol.m^{-3}$
D_{ax}	axial dispersion coefficient	$m^2.s^{-1}$
D_k	Knudsen diffusivity	$m^2.s^{-1}$
D_c	crystal diffusivity	$m^2.s^{-1}$
D_C^0	limiting crystal diffusivity at high temperatures	$m^2.s^{-1}$
D_p	pore diffusivity	$m^2.s^{-1}$
E_a	activation energy of crystal diffusion	$J.mol^{-1}$
H	Henry equilibrium constant	m^3/kg
k_f	film mass transfer coefficient	$m.s^{-1}$
K_L	Langmuir model's constant	kPa^{-1}
K_s	Sips's model constant	kPa^{-n}
L	column's length in the breakthrough experiments	m
M_w	molecular weight	$kg.mol^{-1}$
P	component pressure	kPa
P_p	component pressure in the macropores	kPa
q	adsorbed phase concentration of *i* component	$mol.kg^{-1}$
$\bar{q}$	crystal averaged amount adsorbed phase concentration	$mol.kg^{-1}$
$\langle\bar{q}\rangle$	particle averaged amount adsorbed phase	$mol.kg^{-1}$
q_{max}	maximum adsorbed phase concentration	$mol.kg^{-1}$
q_s	adsorbed phase concentration in the crystals surface	$mol.kg^{-1}$
r_c	crystal radius	m
R_g	ideal gas constant, 8,314 $Jmol^{-1}K^{-1}$	
r_p	mean macropore radious	m

R_p	pellet radius	m
t_{st}	stoichiometric time	s
T	gas temperature	K
u_i	interstitial velocity	$m.s^{-1}$

Greek Letters

ρ_p	adsorbent density	$kg.m^{-3}$
$(-\Delta H)$	isosteric heat of adsorption	$kJ.mol^{-1}$
ε_c	porosity of the column used in the breakthrough experiments	
ε_p	pellet porosity	
τ_p	pore tortuosity	
v_g	Gas kinematic viscosity	$m^2.s^{-1}$

List of Acronyms

GHG	greenhouse gases
MOF	Metal organic frameworks
LNG	liquefied natural gas
NG	natural gas
PSA	pressure swing adsorption
SDA	structure directing agent
TEG	triEthyleneGlycol
TPA	Tetrapropylammonium
XRD	X-ray diffraction.

1 Introduction

1.1 Project's motivation and relevance

Ever since industrial revolution took off, countries have experienced an exponential economic growth, attained by the consumption of fossil fuels at extremely high rates. [1]

Nowadays fossil fuels are used as a primary energy source to reach about 85% of the global energy demand. Their high energy density as well as their accessibility and well known processes of extraction and treatment have made them the key energy source.[2,3]

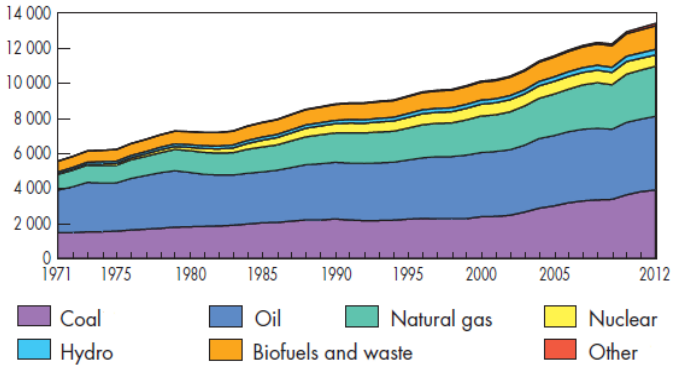

Figure 1 World total primary energy supply from 1971 to 2012 by fuel (Mtoe). Extracted from [4]

The use of fossil fuels explicitly increased the emission of greenhouse effect gases (GHG) such as CO_2 to the atmosphere, accelerating the phenomenom of global warming, causing rapid local and global climate changes. With the industrialization of more countries and the unstoppable population growth, the levels of atmospheric carbon have been rising at a fastest rhythm. The present situation demands an urgent change in electricity production processes as well as, the implementation of CO_2 capture processes. [1-5]

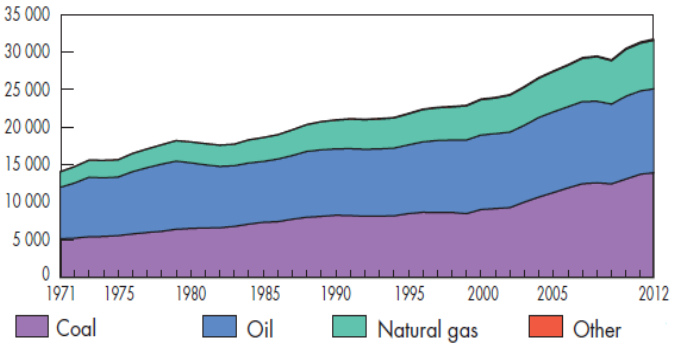

Figure 2 World CO2 emissions from 1971 to 2012 by fuel (Mt of CO2). Extracted from [4]

Consequences of global warming are already felt in countries, such as Norway, by means of climate changes that are affecting wildlife in an irreversible way. Norwegian lifestyle

increased drastically in the past hundred years, mainly caused by the income of the oil and gas industry, however this sector has been the highest source of carbon dioxide emissions since 1990.

In recent years mean temperature has been higher than usual, reaching its highest in 2014, with 2.2ºC above average, however, this tendency is intensified in the Norwegian artic. These higher temperatures have direct consequences in the weather like thaw in the artic and more rain and less snow especially during the winter. Warmer temperatures are causing migration of species, endangering ecosystems that are already vulnerable and threatened. [8-10]

In order to move from an economy powered by fossil fuels to one based on clean energy sources such as solar energy, and wind power, economists, politicians, scientists and engineers need to collaborate, so that new solutions can be developed and new CO_2 emission set-marks can be implemented. New technologies, with higher efficiency and less gas emissions, are continuously emerging and being improved in order to satisfy the world'ss growing energy demand. Taking into account the present technological scenario, the transition to fuels with lower carbon content, complemented with the capture of CO_2, as well as other strategies such as the improvement of energy efficiency and the usage of renewable energies resources, is considered the best option to lower GHG emissions in the next decades. [2, 3]

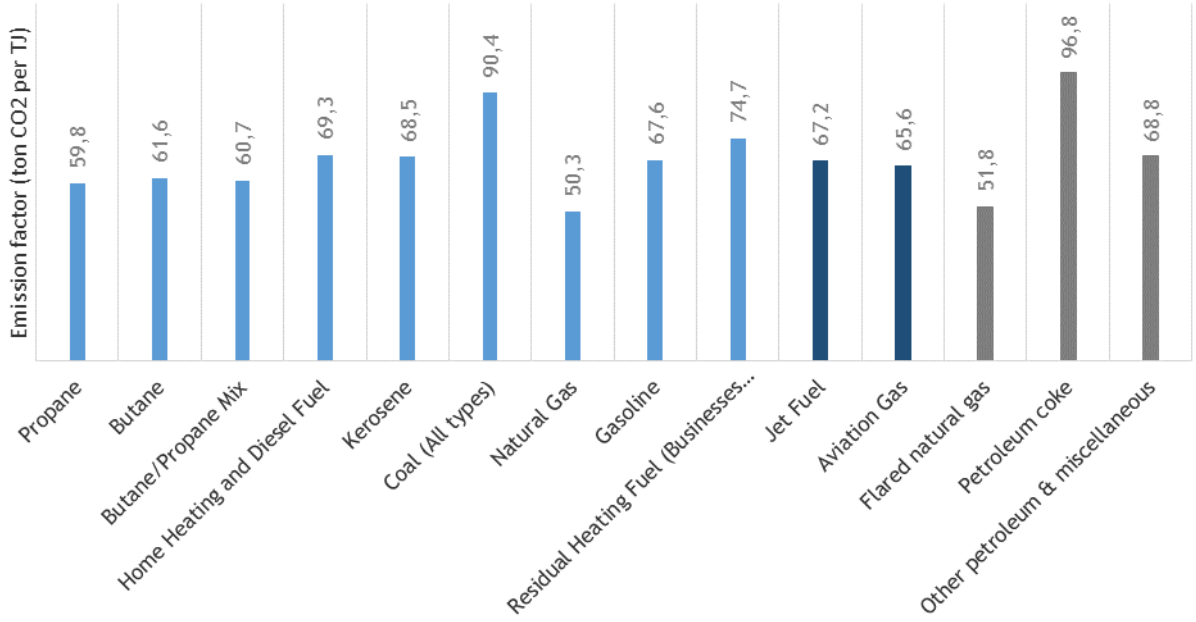

Figure 3 Carbon dioxide emission factor for different fuels. Light Blue (fuels used for homes and businesses); Dark Blue (other transportation fuels); Grey (Industrial fuels and others) [9]

Natural gas (NG) represents a better alternative to other oil derivate products. Being the fossil fuel with less CO_2 emissions when burned (see Figure 3), NG is not only advantageous for the environment but is also economically attractive, since it is cheaper than gasoline or diesel. The NG demand has been increasing rapidly in the last decades, mainly because of the shale gas fracturing expansion phenomenon experienced in this period of time and the continued development of new fracturing technologies, allowing access to resources unreachable until now. Nowadays, not only is this fuel responsible for meeting 25% of the global energy needs in most sectors, such as homes, businesses, vehicles, factories and power plants, but it is also the main feedstock for the chemical industry. Predictions show that the consumption of NG will rise 50% in the next decade. [2, 10-14]

Natural gas (NG) is constituted mainly by methane (CH_4), the hydrocarbon with less carbon content, but it also contains some other higher hydrocarbons (C_{2+}). Furthermore it has impurities such as water, carbon dioxide, nitrogen and hydrogen sulphide, the level of which is characteristic of each geologic formation, and it can vary within the same region. NG is usually classified based on its origin and composition. [2, 15 - 17]

Reservoirs are usually far from the end user, this creates the need for transportation. Depending on the distance and the volume of gas to be transported, the transport of natural gas can be accomplished either by pipelines as a gaseous mixture with at least 75 vol.% of methane or by tankers in form of Liquefied Natural Gas (LNG), containing at least 85 vol.% of methane. In order to meet the transport, and final processing specifications NG has to be treated. The separation processes used depend on the chemical composition of the NG. Water and inert and acid gases are the components that always have to be reduced. Water content reduction is crucial to avoid corrosion, freezing in the cryogenic units, and hydrate formation, and is usually achieved by scrubbing with TriEthyleneGlycol (TEG), followed by adsorption. Inert and acid gases such as carbon dioxide, have no heating value and can lead to steel pipes corrosion and solid formation in the cryogenic equipment. Carbon dioxide is usually removed by a process commonly called gas sweetening, acid gas bulk removal is usually preformed using aqueous amine or organic solvent scrubbing.[18-21]

PSA- Pressure Swing Adsorption is emerging among other gas treating technologies. PSA stands out on the market, since it has low energy consumption, (regeneration does not require heating), and since the adsorbents are regenerated, it doesn't produce chemical residues (unlike the dangerous waste produced by absorption) which makes it eco-friendly. PSA units' sizes are very versatile, making it a great separation technique to be implemented in smaller facilities exploring smaller gas reservoirs. However this sort of technology is still limited by the relatively low adsorptive capacities of the many available adsorbent materials. [17-18,22]

The adsorbent choice is crucial for the well-functioning of the adsorptive technologies. The material choice should satisfy the following requisites: high selectivity, easy regenerability with pressure reduction, high specific capacity, fast diffusion, chemical and physical stability, low cost per volume, and reasonable packing density, to minimize the vessels dimensions. The adsorbent selectivity relays on the difference between the affinity of each species, and the surface of the adsorbent. It usually depends on the difference in adsorption equilibrium (equilibrium selectivity or thermodynamic selectivity) or the difference in adsorption rates (kinetic selectivity).[17]

The separation of carbon dioxide from methane can be achieved based on the adsorbent kinetic selectivity, since both components show great differences in their adsorption rates.

In the present work, Sr^{2+}UPRM-5's kinetic properties were studied, using several methods, to determine its ideal conditions for the kinetic removal of CO_2 from CH_4.

1.2 Outline

This dissertation is organized in five main parts or chapters.

The first chapter elaborated the motivation and relevance of the case study. The modern environmental and social emergency, caused by global warming was highlighted as well as the need to treat natural gas.

The following chapter presents the state of the art, containing the fundamentals for pressure swing adsorption processes, and the presentation of the sorbent studied, with some background on the most recent adsorption technology.

The third part of this document presents the theoretical background of the current work. The point of this chapter was to present fundamentals of the techniques used as well as the models used to fit the experimental data.

In the fourth chapter, all experiments were described and their results are presented and discussed. XRD pattern as well as its lattice parameters were represented, Adsorption isotherms and breakthrough curves are also plotted and fitted to its models.

The final chapter englobes the main conclusions of the thesis.

2 State of the Art

2.1 Sr^{2+}UPRM-5(TPA^{+})

The potential of certain metal organic frameworks (MOF) for PSA have been evaluated, since these materials are highly selective towards CO_2. Only some have been used to separate CO_2/CH_4 mixtures based on its different adsorption rates (kinetics). However, pore size specifications for the kinetic separation of the CO_2/CH_4 mixture can't be attained by most MOFs using simple modification procedures. Some zeolites with pore sizes in the 3–4 Å range, have also been a case study for this type of separation. But their selectivity towards CO_2 is limited, despite of their simple preparation and high working capacities.

A new improvement on the CO_2 selectivity is given by titanium silicate materials, since they are easily modified towards increasing CO_2 selectivity, and they showcase significant pore reduction under thermal dehydration. This contraction leads to reduction of maximum capacity, resulting in more adsorption-regeneration cycles. [14]

Sr^{2+}UPRM-5 is a flexible titanium silicate with enhanced thermal stability range and higher adsorption capacity, without the compromise of the thermal pore contraction property. This material was first developed by Primera-Pedrozo and Hernández-Maldano, and they also discovered that different textural properties and thermal stability could be controlled by changing the structure directing agent (SDA) used. The sample studied in the present work, was synthetized using tetrapropylammonium (TPA^{+}) as a SDA.[13,14,18]

2.2 Pressure Swing Adsorption

Adsorption is a process based on the attraction forces between adsorbent and the species in the fluid. Separation of a gaseous current can be achieved through adsorption, since different species interact differently with the adsorbent phase. By passing a gaseous stream through an adsorbent in a packed bed, the species with less affinity with the adsorbent surface breaks through the column faster, like it happens in a chromatographic column.

The adsorption forces established between the surface of the solid and the gas molecules, are very weak, allowing the regeneration of the adsorbent by simply changing one of the operating conditions (feed concentration, pressure or temperature). The functioning of a PSA unit can be summarized in two steps. The first one is the adsorption phase, during this step the gas mixtures is in contact with the adsorbent at relatively high pressures, producing a gas stream rich in the less adsorbed species (the raffinate). After certain established time the bed is almost saturated, and the second step begins, the regeneration phase. By lowering

pressure, the, strongly adsorbed components are released from the adsorbent (the extract) making it clean and ready for the adsorption phase again.

In order to maximize productivity and energy saving, several columns are operated in a swing mode, making the process continuous. Other steps were added to the simple cycle, one of these is the purge step, in which adsorbent regeneration is increased by recycling the raffinate. A complete cycle lasts minutes or seconds, and is operated at isothermal conditions.

NG is often obtained at high pressures. PSA processes seem very attractive to produce methane at high pressure as a raffinate, not only purifying it but also reducing further compression.[18]

PSA is already implemented vastly in areas such as hydrogen purification from steam methane reforming, drying and air separation (oxygen and nitrogen capture). However it still has some limitations (as mentioned in the last section) that require the attention of fields such as material science and engineering to be overcome.

3 Theoretical Background

3.1 X-Ray Powder Diffraction (XRD)

X-Ray diffraction is an analytical technique used for the study of crystalline materials' phases, as well as the dimensions of their unit cell. In this analysis the sample must be grinded until it becomes a fine, homogeneous powder. X-Ray diffraction is based on the constructive interference of the monochromatic x-rays with the crystalline sample. The x-rays are generated in a cathode ray tube, then filtered, in order to produce monochromatic radiation, collimated to concentrate and directed to the sample. When this monochromatic beam hits the sample, in Bragg's law (equation 1) satisfactory conditions, it produces a constructive interference (diffracted ray).

$$n\,\lambda = 2\,\mathrm{d}\,\sin\theta \tag{1}$$

Bragg's Law relates the radiation wavelenght with the obtain diffraction angle and the lattice spacing of the sample. The diffracted rays are detected, gathered, and counted. When the sample is scanned through a range of 2Θ angles, all possible diffraction directions of the lattice are attained due to the random orientation of the powdered material. Diffraction's key component is the angle between the incident and diffracted rays. Conversion of the diffraction peaks to d-spacings makes the mineral identification possible. The identification process is made by comparison of d-spacings with standard reference patterns, since each mineral as a unique d-spacings set. [23]

3.2 Adsorption equilibrium

Adsorption equilibrium is considered the dynamic state established between the molecules in the fluid phase and the ones in the adsorbed phase at a certain temperature and fluid concentration.

Adsorption equilibrium isotherm represents the amount of a component that is in the adsorbed phase as a function of the amount of the same component present in the fluid, when both phases are at equilibrium at a certain temperature.

3.2.1 Langmuir Model

From a large number of existing models the Langmuir model is the simplest to describe monolayer adsorption.

The model is based on the assumptions that the adsorbent has a certain number of well-defined localized sites, each of which is able to accommodate only one adsorbate molecule. It

also considers that the adsorption energy is constant and equal in all sites and that there is no lateral energetic interference between other adsorbed molecules nearby. [24]

The following equation represents the Langmuir model

$$q = \frac{q_m K_L P}{1+K_L P} \quad (2)$$

where q is concentration of adsorbate in the solid phase, q_m represents the saturation capacity of the adsorbate, K_L is the adsorption constant and P is the adsorbate partial pressure in the fluid phase.

3.2.2 Sips Model

The Sips model is a result of the combination of the Langmuir and Freundlich isotherms and is described as follows

$$q = \frac{q_m K_S P^n}{1+K_S P^n} \quad (3)$$

where K_s and n are constants that are temperature dependent.

At low pressures the sips model can be reduced to the Freundlich form and at higher pressure range, it approaches the capacity of the Langmuir model.[25]

3.3 Adsorption kinetics

When a system is in equilibrium and a perturbation is induced, the molecules experience a net driving force moving them to another equilibrium state, and this takes a certain time. In order to adsorb, the molecules have to overcome a series of resistances from the bulk to the adsorption sites. From the bulk phase, molecules have to reach the inner part of the pellets, sometimes going through a film resistance formed in the outside of the particle, once they reach the inside, they have to diffuse into the macropores (macropore diffusion resistance) finding a perfect place to adsorb.

In a bidisperse adsorbent, such as Sr^{2+}UPRM-5 the majority of the molecules is adsorbed in the crystal, which means that sometimes they have to go through an additional resistance, the diffusion in the micropores to the adsorption sites.

Diffusion rates are dependent on the similarity between the pore mouth size and the molecular diameter and on the interactions between the adsorbent and the adsorptive. Meaning that if a molecule diameter is smaller than the pore mouth, will be easier adsorbed than a molecule with a size comparable or higher than the pore mouth. Although methane is a bigger molecule than the carbon dioxide, in equilibrium-based materials diffusion of carbon dioxide tends to be lower than methane because of interactions with the surface. [17,26]

3.4 Dilute breakthrough curves

Breakthrough curves can be used to measure equilibrium and kinetics when the amount adsorbed is very small or when the adsorption kinetics is very fast. In this technique, a step gradient in the concentration is imposed into a packed bed column. The adsorption kinetics and equilibrium can be calculated from the continuous measurement of outlet concentration of the column.

Since the step component concentration imposed is extremely diluted (0.5%) it assures that the adsorption equilibrium occurs under linear conditions and that the gas velocity can be considered constant in the entire column.

In order to have a better understanding of the dynamics of the studied adsorption process, a model was developed.

The following equations describe the behaviour of a fixed-bed packed with a bidisperse adsorbent, with axial dispersed flow. Besides the macropore and micropore resistances the model also includes the possibility of a film resistance in the external surface of the pellets.[26]

The mass balance to a differential element of the packed column is described as follows (Ruthven, 1984):

$$\frac{\partial C}{\partial t} + \left(\frac{1-\varepsilon_c}{\varepsilon_c}\right)\varepsilon_p \frac{\partial \langle C \rangle}{\partial t} + \left(\frac{1-\varepsilon_c}{\varepsilon_c}\right)\rho_p \frac{\partial \langle \bar{q} \rangle}{\partial t} = D_{ax}\frac{\partial^2 C}{\partial z^2} - u_i \frac{\partial C}{\partial z} \quad (4)$$

The initial and boundary conditions considered to solve the equation are presented below.

Initial conditions:

$$C_{(0,z)} = 0 \quad (5)$$

Boundary Danckwerts conditions:

$$D_{ax}\frac{\partial C}{\partial z}\Big|_{(t,0)} = u_i(C - C_0) \quad (6)$$

$$\frac{\partial C}{\partial z}\Big|_{(t,L)} = 0 \quad (7)$$

where ε_c represents the porosity of the column, ε_p the porosity of the pellet, $\langle C \rangle$ is the particle-averaged concentration in the macropores of the pellet (extrudate) and is obtained using equation 8, ρ_p is the adsorbent density, $\langle \bar{q} \rangle$ is the particle averaged adsorbed phase concentration, D_{ax} is the axial dispersion coefficient, and finally u_i is the interstitial velocity.

$$\langle C \rangle = \frac{2}{R_p^2}\int_0^{R_p} C_p R \, dR \quad (8)$$

The diffusion in a slab zeolite crystal (microporous) is described by Fick:

$$\frac{\partial q}{\partial t} = D_c \frac{\partial^2 q}{\partial r^2} \tag{10}$$

D_c is the crystal diffusivity. Solving this differential equation is only possible with help of the following initial and boundary conditions.

$$q_{(r,0)} = 0 \tag{11}$$

$$\left.\frac{\partial q}{\partial r}\right|_{(0,t)} = 0 \tag{12}$$

$$q_{(r_c,t)} = q_s = f(C_p) \tag{13}$$

The last condition is the condition of equilibrium at the crystal surface. As mentioned before the adsorption equilibrium is considered linear throughout all the experimental run.

$$q_s = HP_p \tag{14}$$

q_s is the adsorbed phase concentration in the crystal surface, H is the Henry equilibrium constant and P_p is the pressure of hydrocarbon in the macropores.

The micropore diffusivity has an exponential dependence with the temperature described by Arrhenius in the following way:

$$D_c = {D_c}^o e^{-\frac{E_a}{R_g T}} \tag{15}$$

where ${D_c}^o$ represents the limiting diffusivity, E_a the activation energy and R_g is the universal gas constant.

The mass balance in a volume element of the extrudate is represented by the following expression

$$\varepsilon_p \frac{\partial C_p}{\partial t} + \rho_p \frac{\partial \bar{q}}{\partial t} = \frac{1}{R}\frac{\partial}{\partial R}\left(\varepsilon_p D_p R \frac{\partial C_p}{\partial R}\right) \tag{16}$$

The initial and boundary conditions to solve the equation are

$$C_{p\,(R,0)} = 0 \tag{17}$$

$$\varepsilon_p D_p \left.\frac{\partial C_p}{\partial R}\right|_{(R_p,t)} = k_f (C - C_p)_{(R_p,t)} \tag{18}$$

$$\left.\frac{\partial C_p}{\partial R}\right|_{(0,t)} = 0 \tag{19}$$

D_p is the pore diffusion coefficient, C_p is the gas concentration in the macropores and is related to the pressure of hydrocarbon in the micropores by the ideal gas equation (equation 20), R_p is the pellet radius and k_f is the film mass transfer coefficient in the external surface of the extrudate.

$$P_p = C_p R_g T \tag{20}$$

Pore diffusivity is a function of the molecular and Knudsen diffusion:

$$\frac{1}{D_p} = \frac{\tau_p}{D_m} + \frac{\tau_p}{D_K} \tag{21}$$

$$D_K = 0.97 r_p \sqrt{\frac{T}{M_w}} \tag{22}$$

where τ_p is the pellet's tortuosity, M_w is the molecular weight of the hydrocarbon, r_p is the pore radius, D_K is the Knudsen diffusivity, and D_m is the molecular diffusivity, that is given by the Chapman-Enskog equation.

In order to solve the model described above some parameters had to be calculated such as axial diffusion coefficient and the film mas transfer coefficient (Ruthven,1984):

$$D_{ax} = (0.45 + 0.55\varepsilon_c) D_m + \gamma_2 2 R_p u_i \tag{23}$$

where γ_2 has the value of 0.5.

In order to obtain the film mass transfer coefficient, the Wakao and Funazkri correlation was used:

$$Sh = 2.0 + 1.1\, Sc^{\frac{1}{3}} Re^{0.6} \tag{24}$$

where the dimensionless variables are given by:

$$Re = \frac{u_i d_p}{\vartheta_g} \tag{25}$$

$$Sc = \frac{\vartheta_g}{D_m} \tag{26}$$

$$Sh = \frac{2 R_p k_f}{D_m} \tag{27}$$

ϑ_g is the kinematic viscosity of the gas and d_p is the pore diameter.

The model was implemented in the *gPROMS* software, and fitted to the experimental data, allowing the calculation of the parameters that provide the better fitting, with an acceptable error.

4 Experimental

4.1 Characterization

In situ X-ray diffraction characterization of Sr-UPRM-5 was performed on a Panalytical Empyrean X-ray powder diffractometer (PANalytical B.V., the Netherlands) equipped with an Anton Paar XRK 900 (Anton Paar GmbH, Austria) *in situ* high temperature (25-900 °C) and high pressure (1-10 bar) reactor cell. Data were collected stepwise over the 2θ range 4 – 50 °, with a step size of 0.01° and a scan speed of 0.08 °/s, using $Cu_{K\alpha}$ radiation (λ = 1.54187 Å). The sample was heated up stepwise under vacuum in the *in situ* cell with a heating rate of 1 K/min. When reaching the desired activation temperature (25, 50, 75, 100, 125, 150, 175, 200, 225, 250, 275 and 300 °C), it was kept there for 30 min and then cooled down to 25 °C, where the XRD pattern was recorded, before heating up the sample to the next activation temperature.

Figure 4 High pressure reactor cell with sample

The XRD patterns were recorded at 25 °C between each activation step in order to avoid having an effect of thermal expansion, and to be able to observe the actual change in the unit cell as a function of activation temperature.

4.2 Adsorption Equilibrium at Low Pressures

Adsorption equilibrium isotherms where measured using a Belsorp-Max Instrument (BEL JAPAN) at 25 ºC. The gases used for the measurement were CO2 (purity >99.995%) and CH4 (purity >99.995%). After being deposited in the sample holder, vacuum was applied to the sample. The sample activation was done overnight, using a heat ramp of 2 ºC/min to the desired temperature. The activation temperatures chosen were 80, 90, 100, 110 and 120 ºC. Considering that the CH4 molecule would have more trouble adsorbing than the CO2, it was

determined that the adsorption equilibrium was measured after 10000s and 300s within 0.3% of pressure change respectively.

Figure 5 Experimental Setup

4.3 Diffusion Experiments

Two different types of breakthrough experiments (methods A and B) were carried out in order to obtain the diffusive resistance of a diluted gas current in a Sr2+URPM-5 sample.

The sample was packed in a very small column placed in a gas chromatograph, HP6890 (GIM). Sample activation was made overnight using a heating ramp of 2ºC/min up to the desired temperature. The activation temperatures analysed, using the two methods, were 80, 90, 100, 110 and 120ºC. A step gradient is imposed in the inlet gas current, and the outlet gas stream is analysed by a Thermal Conductivity Detector (TCD). Because of the small size of the column a very small flow rate was used in all experiments, of about 10.0 ± 0.1 ml/min.

A list of the operating conditions used in this tests is presented in Table 3. In the beginning of each experiment the sorbate was clean of adsorptive, this was achieved either by sample activation or by passing a current of nearly pure helium for as long as it took to lower the signal to its baseline (this time depended on the system temperature and the inlet flow rate). Before each experiment, the GC's oven temperature was set for 30 min, to assure that the column's temperature is homogeneous.

Table 1 Operating conditions used for breakthrough experiments

Adsorptive concentration	0.5% v/v
Mass of adsorbent (g)	0.2419
Adsorbent density (assumed) (g/cm^3)	1.0
Column length (cm)	3.8
Column diameter (cm)	0.43
Column porosity (assumed)	0.4
TCD temperature (°C)	150
TCD Reference flow rate (cm^3/min)	15

The signal generated in the TCD was normalized and that way the breakthrough curve was obtained for each test.

Stoichiometric time was calculated from the experimental data using the following expression (Ruthven, 1984):

$$t_{st} = \frac{L_c}{u_i}\left[1 + \left(\frac{1-\varepsilon_c}{\varepsilon_c}\right)H\right] = \int_0^\infty \left(1 - \frac{C}{C_0}\right)dt \quad (28)$$

The same equation relates the stoichiometric time with the Henry's constant. Allowing the calculation of the components amount adsorbed.

Figure 6 Column used during breakthrough experiments. Pencil used for scale

5 Results and Discussion

5.1 Characterization

Comparing the XRD patterns represented in the figure above, at higher temperatures, a slight shift of the peaks is noticed towards the higher 2Θ values, indicating a reduction in the lattice parameters of the unit cell. Increasing loss of the sample's crystallinity also occurs with the heating at increasing temperature.

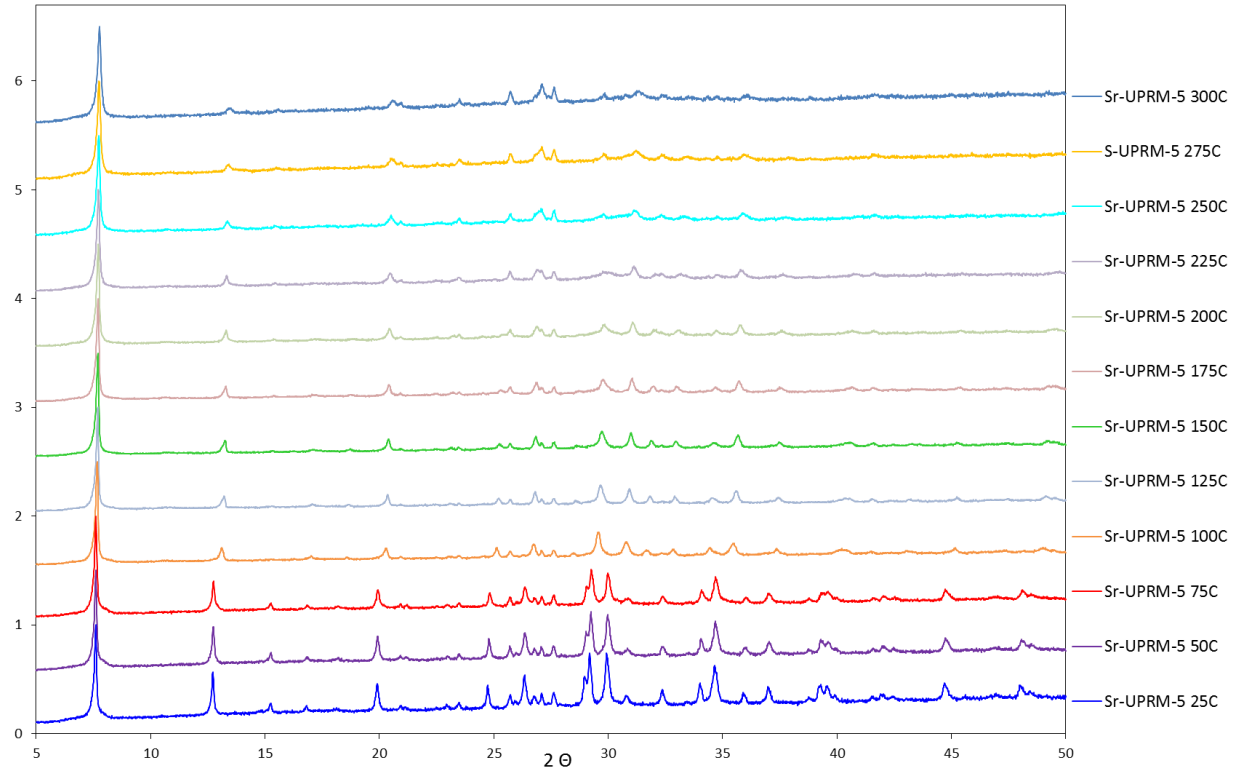

Figure 7 XRD pattern of Sr^{2+}UPRM-5 heat treated at various temperatures looking at the changes in peak position in the 2Θ range.

From the XRD data, the lattice parameters were calculated (see Figure 5) showing the structure reduction with increasing temperature. This framework contraction is higher between 75 and 100 ºC and accentuated in the *c* parameter. The lattice parameter c is considered to be associated with 8-member ring (8-MR) pores or channels.[14,18] These types of pores are believed to dominate gas adsorption kinetics, since they can be tailored in another adsorbent, Sr^{2+}ETS-4, to separate gas molecules of similar sizes.[14]

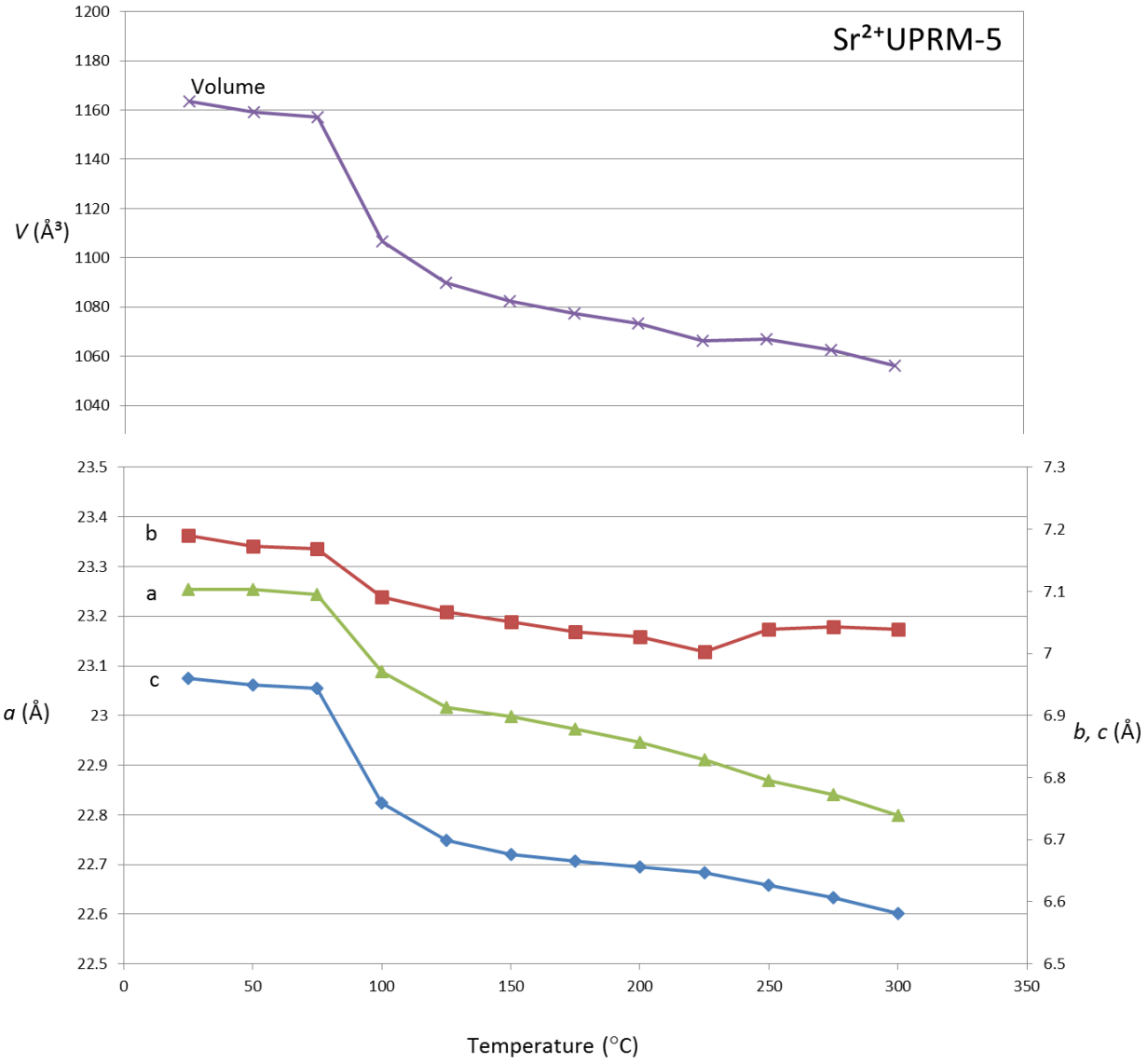

Figura 8 Changes in the lattice parameters for Sr^{2+}UPRM-5 at different activation temperatures

The unit cell volume was also calculated and it seems to change according to the c parameter. Between 75 and 100 ºC showed a higher unit cell volume reduction of 4.3%, considering that the total reduction is of 9.2%. If 8-MR pores are able to control access to the adsorbent framework, the best molecular gate effect should be found when the sample is activated at temperatures between 75 and 100 ºC. From these temperature ranges, 80, 90 and 100 ºC where initially chosen to be activation temperatures to study.

5.2 Adsorption Equilibrium at Low Pressures

Maximum carbon dioxide adsorption capacity recorded at 100 kPa was ca.1.70mmol.g^{-1} after activation at 110ºC, even though a similar yet slightly smaller value was attained when the sample was activated at 120ºC.

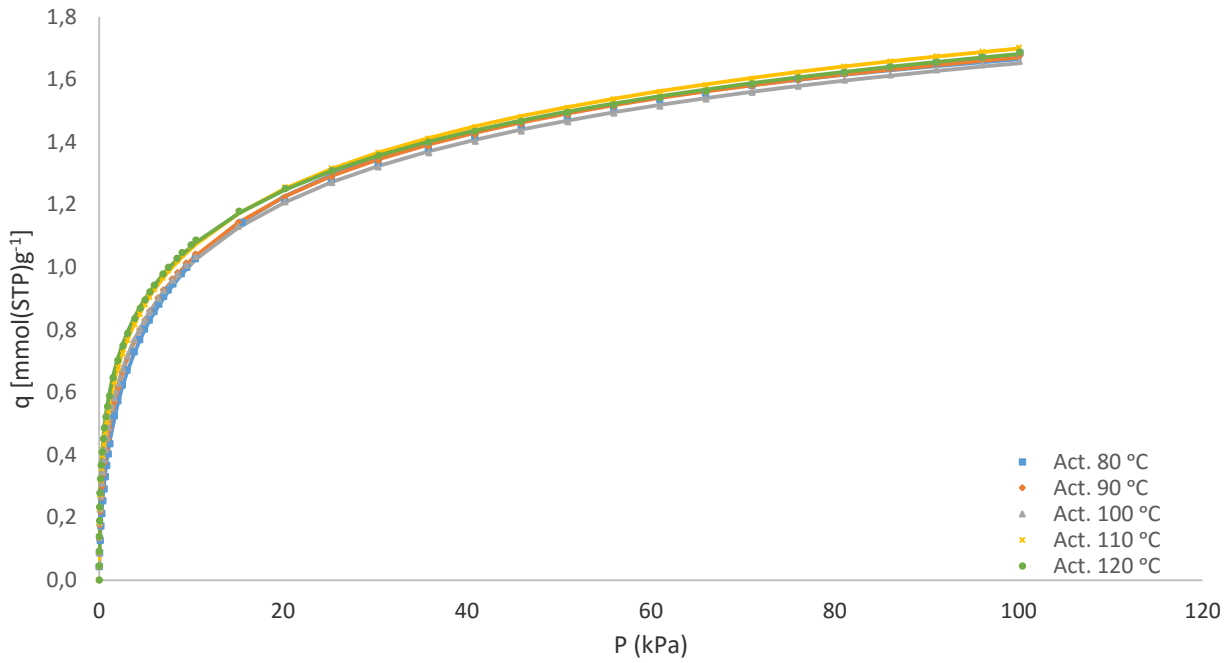

Figure 9 Adsorption isotherm of CO_2 at 298K after activation at several temperatures. The points represent the experimental data and the lines the Sips fit

From the analysis of the several CO_2 isotherms it's observed that in the lower pressure range (<1kPa) the adsorptive amount increases with higher activation temperature. This changes with higher pressures, and near 20 kPa, higher adsorbed amounts were obtained in the sample activated at 110ºC instead of 120ºC. This change in behaviour at higher pressures, might result of water elimination from the silicate structure and contraction of the structure demonstrating the results obtained by the XRD characterization.

It's also impossible to determine the better Temperature for activation, since in changes with gas pressure. The choice is different depending in what is the pressure range that is being studied.

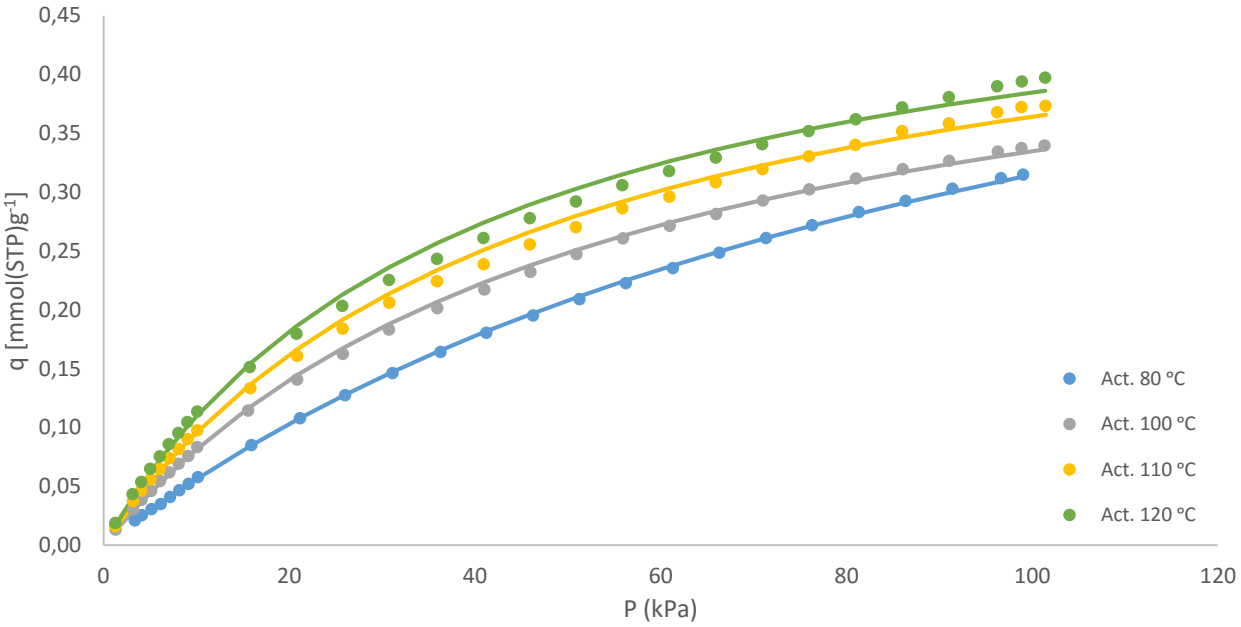

Figure 10 Adsorption isotherm of CH_4 at 298K after activation at several temperatures. The points represent the experimental data and the lines the Sips fit

Maximum methane adsorption capacity recorded at 100 kPa were ca.0.40 mmol.g^{-1} after activation at 120ºC.

Higher adsorbed amount values were obtained when adsorbing CO_2 showing the adsorbent preference towards this gas.

The amount of methane increases with temperature, and if the pore sizes are being reduced (as expected) the only explanation would be that surface area would increase, however without any additional tests none of this can be concluded.

The isotherms of carbon dioxide and methane were fitted to the Langmuir model (equation 2) and its parameters are represented in Table 2. Std. deviation values, indicate that the Langmuir model is not a good representative of the adsorption equilibrium, especially on the CO_2 case. The experimental data were afterwards fitted to the Sips model (equation 3), its parameters are represented in Table 3.

Table 2 Langmuir Parameters of CO_2 and CH_4 isotherms after activation at several temperatures

Adsorptive	Activation temperature (ºC)	Mass of adsorbent (g)	q_m (mmol.g^{-1})	K_L (kPa)$^{-1}$	Std.Dev [1]
CO_2	80	0.08158	1.70	2.11 x 10^{-1}	±0.092
	90	0.08158	1.68	2.47 x 10^{-1}	±0.113
	100	0.08158	1.65	2.58 x 10^{-1}	±0.122
	110	0.07772	1.69	2.83 x 10^{-1}	±0.137
	120	0.07712	1.67	3.09 x 10^{-1}	±0.148
CH_4	80	0.08158	0.646	9.50 x 10^{-3}	±0.001
	90	0.08690	0.285	2.23 x 10^{-2}	±0.008
	100	0.08158	0.513	1.88 x 10^{-2}	±0.003
	110	0.07722	0.529	2.20 x 10^{-2}	±0.006
	120	0.07682	0.534	2.58 x 10^{-2}	±0.007

The Sips isotherm seems to be a better representative of the experimental CO_2 adsorption equilibrium data. Methane experimental data is also described by the Sips model but with n=1, in this case describing the Langmuir's monolayer adsorption. This might happen since the attraction forces between the adsorbent surface and the CH_4 molecules are weaker than the CO_2, and there is no considerable intermolecular interaction.

Theoretically the q_m parameters should be constant for each gas, and K_L would lower with temperature. This does not occur with methane at 100, 110 and 120ºC.

[1] Standard deviation was calculated based on residuals between the observed data and the calculated equilibrium loading amounts for the complete pressure range.

Table 3 Sips Parameters of CO_2 and CH_4 isotherms after activation at several temperatures.

Adsorptive	Activation temperature (°C)	Mass of adsorbent (g)	q_m (mmol.g^{-1})	K_L (kPa)$^{-1}$	n	Std.Dev[1]
CO_2	80	0.08158	2.20	2.31×10^{-1}	0.6	0.0090
	90	0.08158	2.42	2.40×10^{-1}	0.5	0.0046
	100	0.08158	2.59	2.34×10^{-1}	0.4	0.0050
	110	0.07772	2.83	2.38×10^{-1}	0.4	0.0065
	120	0.07712	3.01	2.38×10^{-1}	0.4	0.0065
CH_4	80	0.08158	0.646	9.50×10^{-3}	1	±0.001
	90	0.08690	0.285	2.23×10^{-2}	1	±0.008
	100	0.08158	0.513	1.88×10^{-2}	1	±0.003
	110	0.07722	0.529	2.20×10^{-2}	1	±0.006
	120	0.07682	0.534	2.58×10^{-2}	1	±0.007

5.3 Diffusion Experiments

5.3.1 Method A – Breakthrough Curves

This method is the traditional breakthrough experiment, in which, a step perturbation is imposed in the inlet gas current, and the outlet current is continuously measured. During this stage the sample would have reached its maximum adsorptive capacity, at this point the equilibrium between both phases is established. Desorption of the column is attained by setting the component concentration, in the inlet current, instantaneously to zero again, until the outlet currents signal reaches the baseline. For each component studied, the chosen measured temperatures were 26, 40 or 70ºC. All tests were made under isothermal conditions. In fact the inability to maintain the GC under isothermal condition at 25ºC, made it impossible to collect experimental data at this temperature. In this case an approximate temperature was chosen (26ºC). This approximation enables the comparison with other data collected at 25ºC.

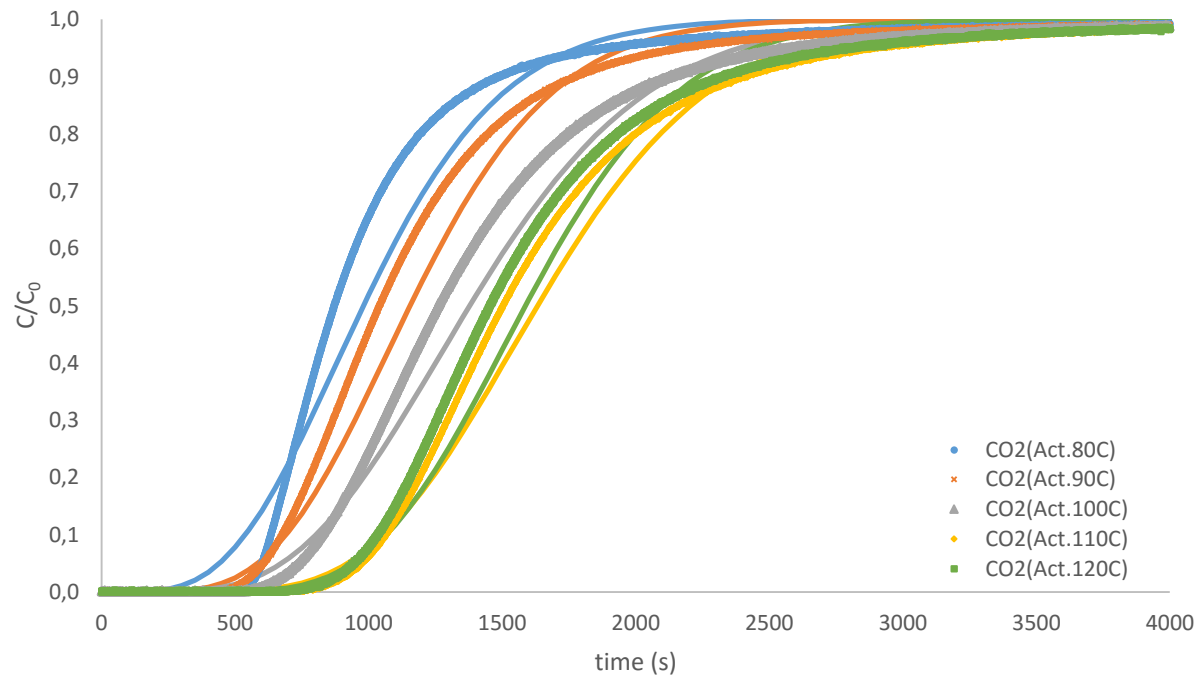

Figure 11 Breakthrough curves of CO_2 at 26ºC for different activation temperatures. The points represent the experimental data and the lines the model

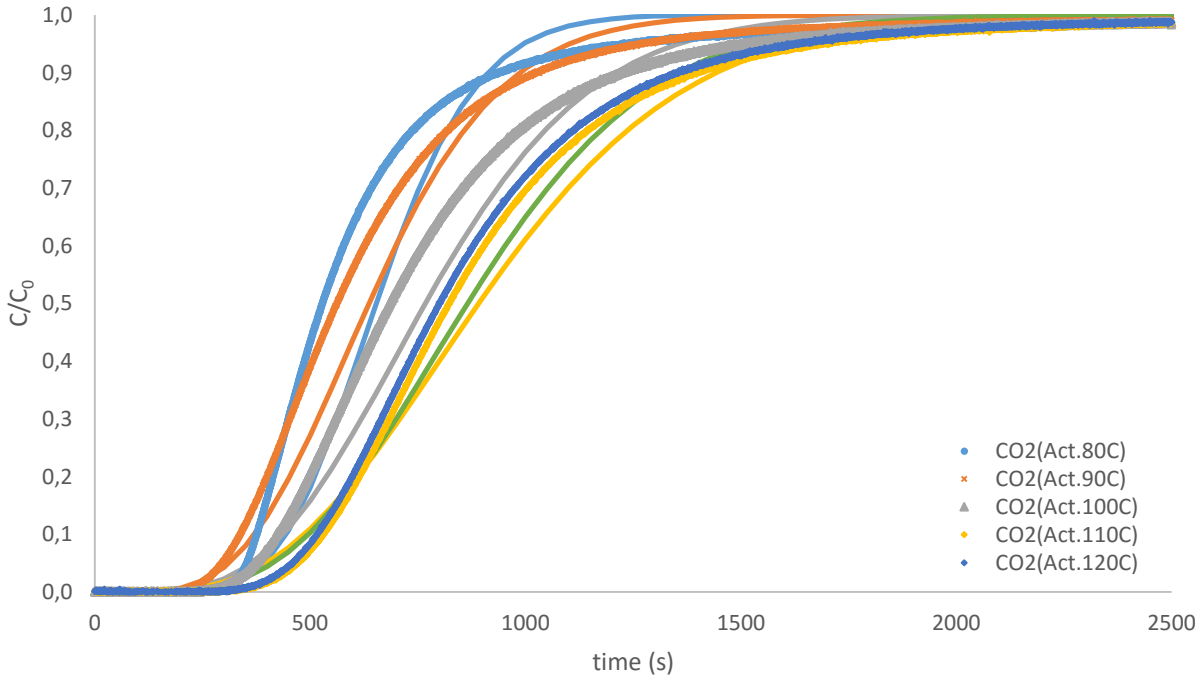

Figure 12 Breakthrough curves of CO_2 at 40ºC for different activation temperatures. The points represent the experimental data and the lines the model

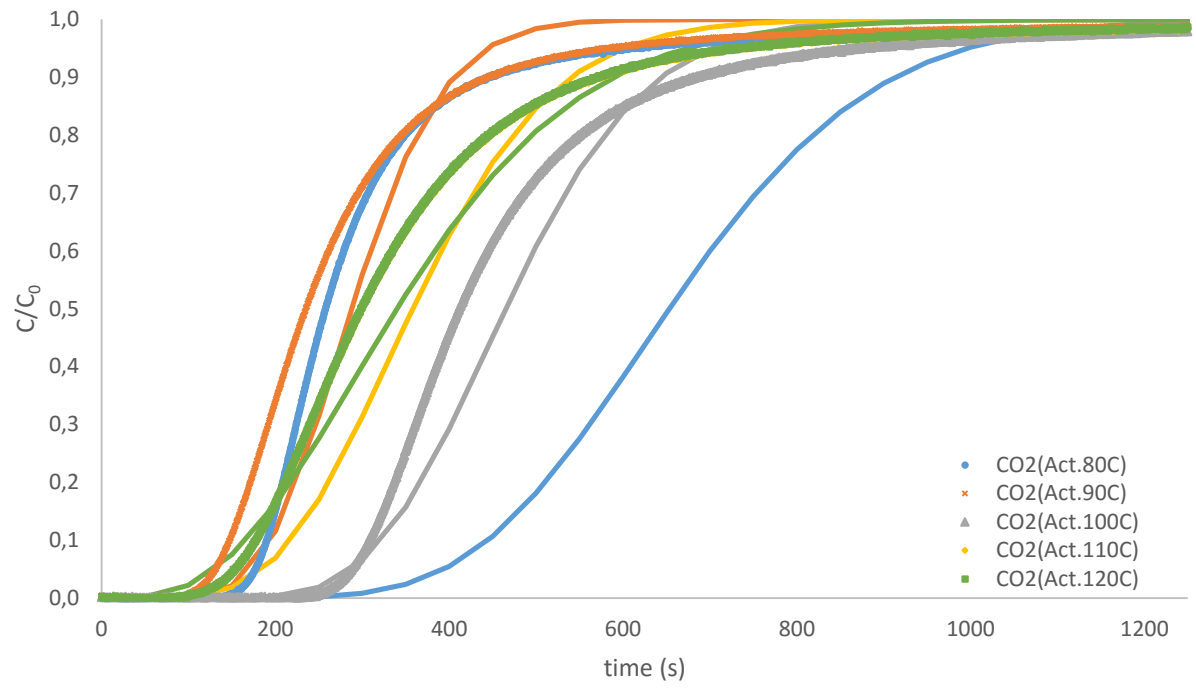

Figure 13 Breakthrough curves of CO_2 at 70ºC for different activation temperatures. The points represent the experimental data and the lines the model

For each breakthrough curve of CO_2, the higher value of stoichiometric time was observed in the sample activated at 110ºC, independently of the temperature at which the measurements took place. For each activation temperature, the stoichiometric time decreased with increasing temperature, this is justified since the adsorption is a favourable process at lower temperatures.

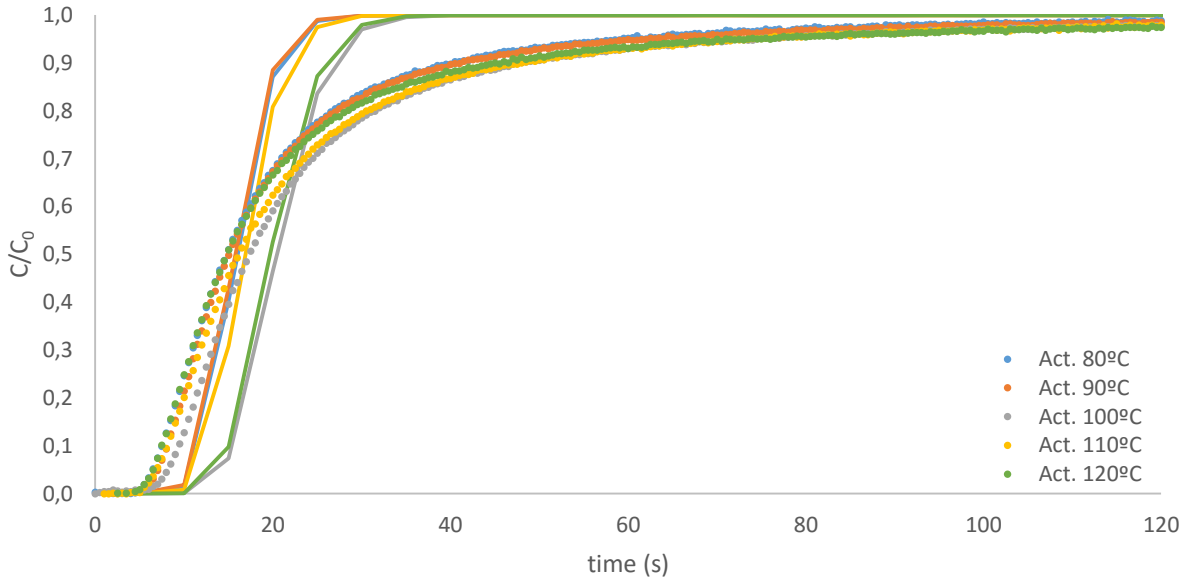

Figure 14 Breakthrough curves of CH_4 at 26ºC for different activation temperatures. The points represent the experimental data and the lines the model

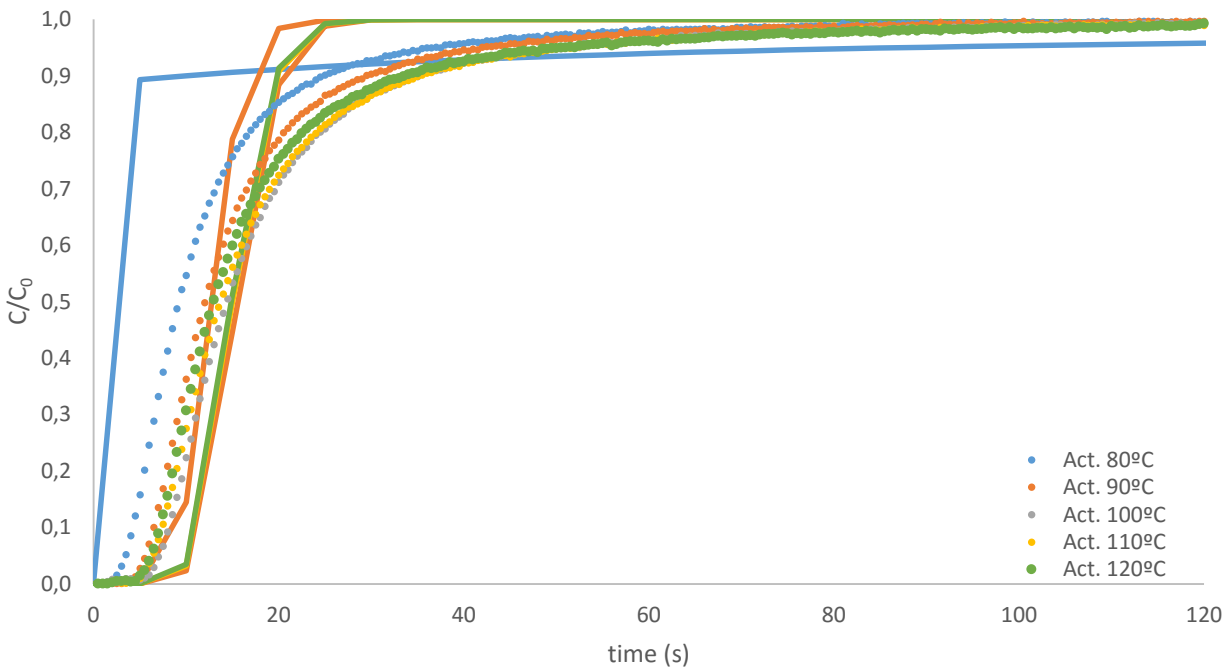

Figure 15 Breakthrough curves of CH_4 at 40ºC for different activation temperatures. The points represent the experimental data and the lines the model

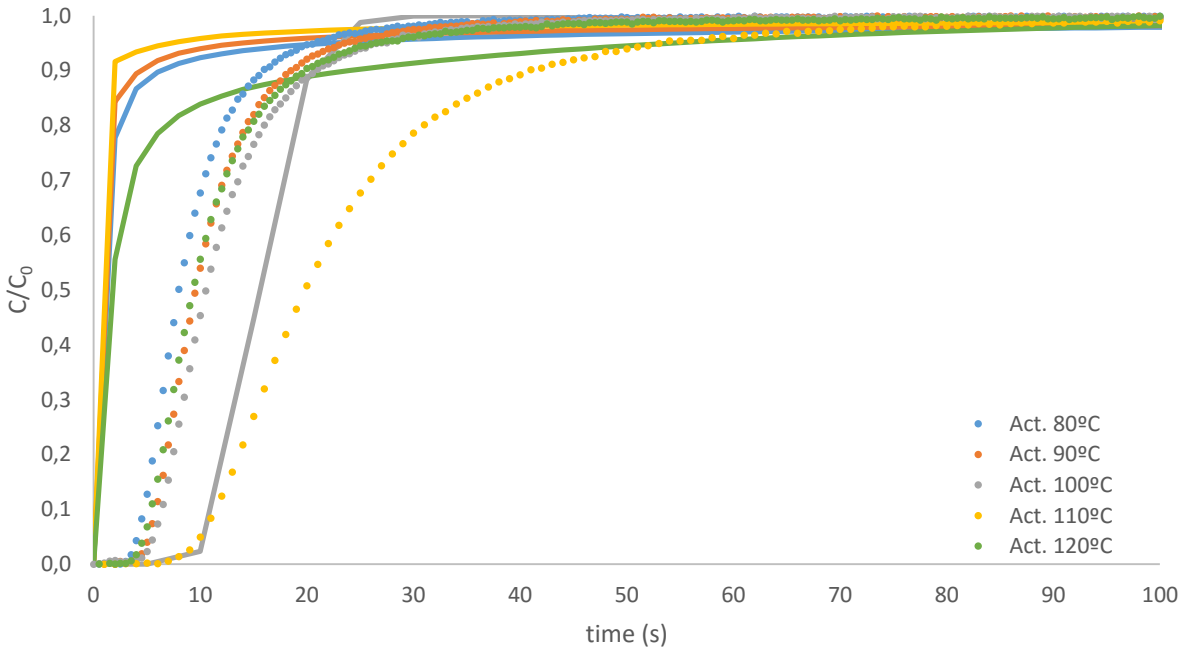

Figure 16 Breakthrough curves of CH_4 at 70ºC for different activation temperatures. The points represent the experimental data and the lines the model

Unlike the carbon dioxide, methane breaks through the column almost instantaneously. This reinforces the idea that methane, being larger than CO_2 has more trouble diffusing in the pore mouths, and reaching the preferable adsorptive sites.

In the methane case, the stoichiometric time didn't vary much for each activation temperature, assuming slightly higher values for the sample activated at 100 ºC. Stoichiometric time showed the same tendencies with increasing temperature as seen on the CO_2 measurements.

Most simulations obtained with gPROMS software should be repeated once that in the methane experiments the fitting is not as expected.

The stoichiometric times, Henry's constants, and heats of adsorption calculated for each breakthrough experiment are organized in tables 5 and 6.

5.3.2 Method B – Temperature Programmed Desorption Breakthrough Curves

This breakthrough experiments are very similar to the ones studied with method A. GC's oven was set to 26ºC, and a step gradient of concentration was imposed in the inlet gas current. When the signal reaches its maximum and stabilizes, the temperature in the GC was set to 40 ºC and it would stay in that value until the system would reach its stable state again, at this point the GC's temperature was set to 70 ºC until the system would stabilize again. At this point the concentration in the inlet current would be set again to zero, desorbing the column. During the tests the outlet current was being continuously monitored.

Since UPRM-5 is considered a kinetic adsorbent, the time that takes from the temperature change to system equilibrium is extremely small. In the exact moment that each temperature disturbance is imposed, the system was at equilibrium and the feed concentration didn't suffer any changes. This disturbance forces the adsorbed molecules to move to another state of equilibrium, and this molecule movement is detected in the signal as a peak. Since any other parameter stays constant, this peak is quantification of the diffusion in the pores.

In the CO_2 experiments, the signal had to be slightly attenuated due to the high signal values achieved during the experiment, that otherwise couldn't be detected. In all the CO_2 experiments a range of 2 was used.

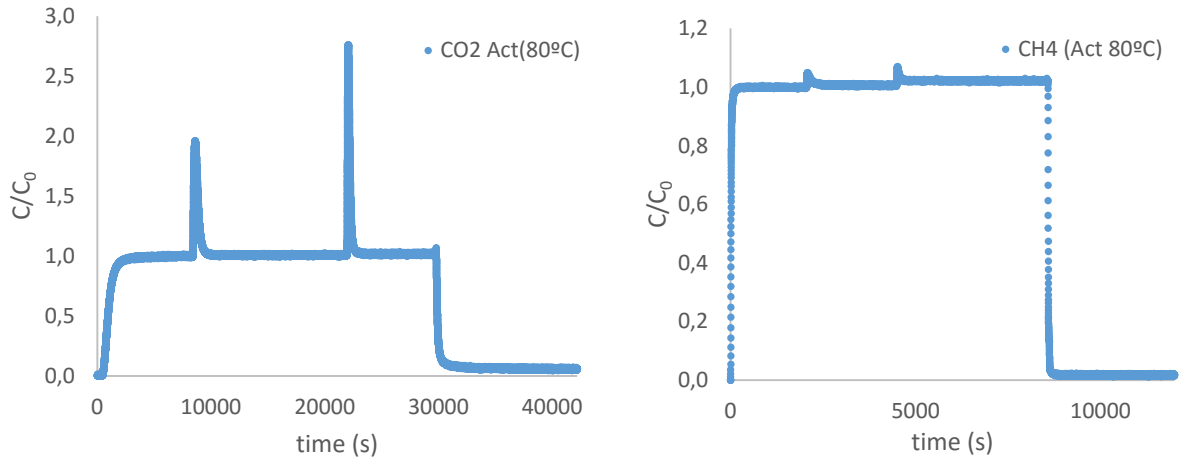

Figure 17 Breakthrough curves obtained using Method B using a UPRM-5 sample activated at 80ºC

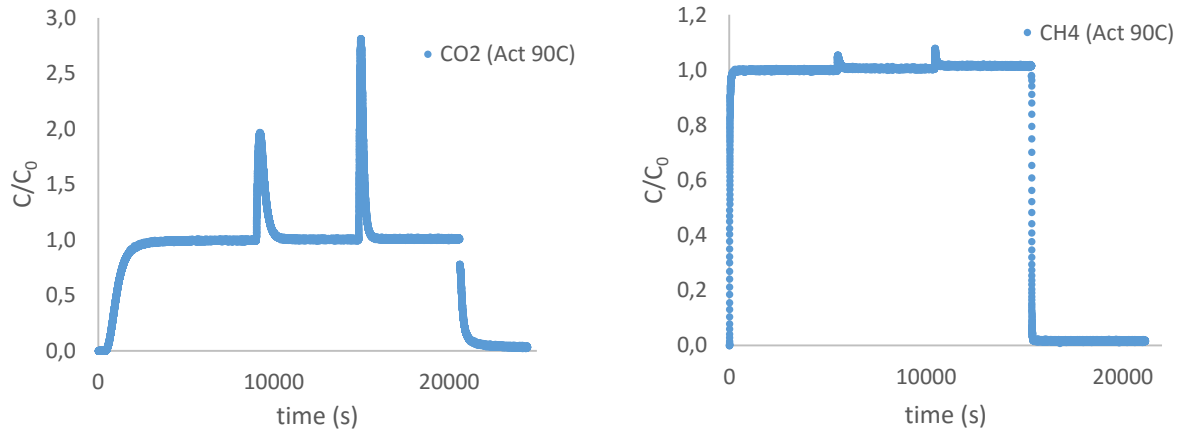

Figure 18 Breakthrough curves obtained using Method B using a UPRM-5 sample activated at 90ºC

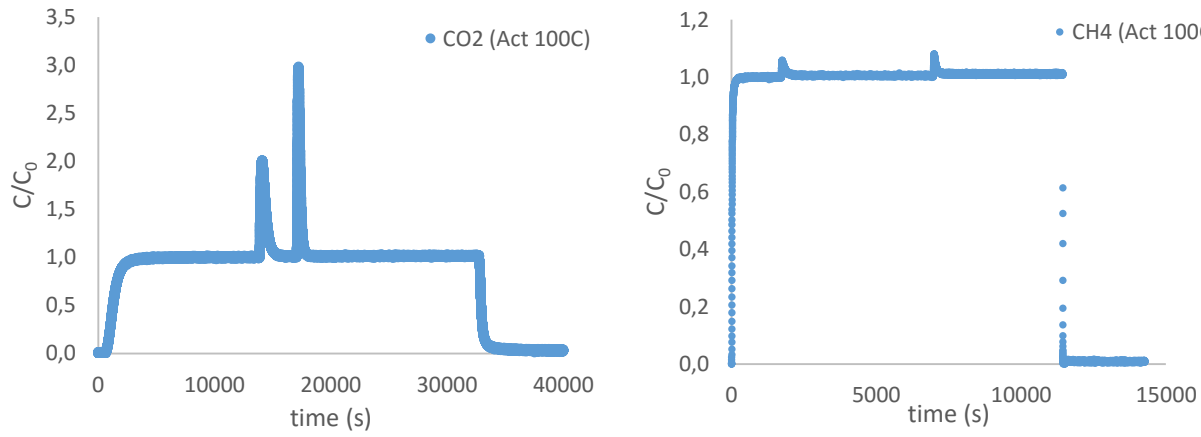

Figure 19 Breakthrough curves obtained using Method B using a UPRM-5 sample activated at 100ºC

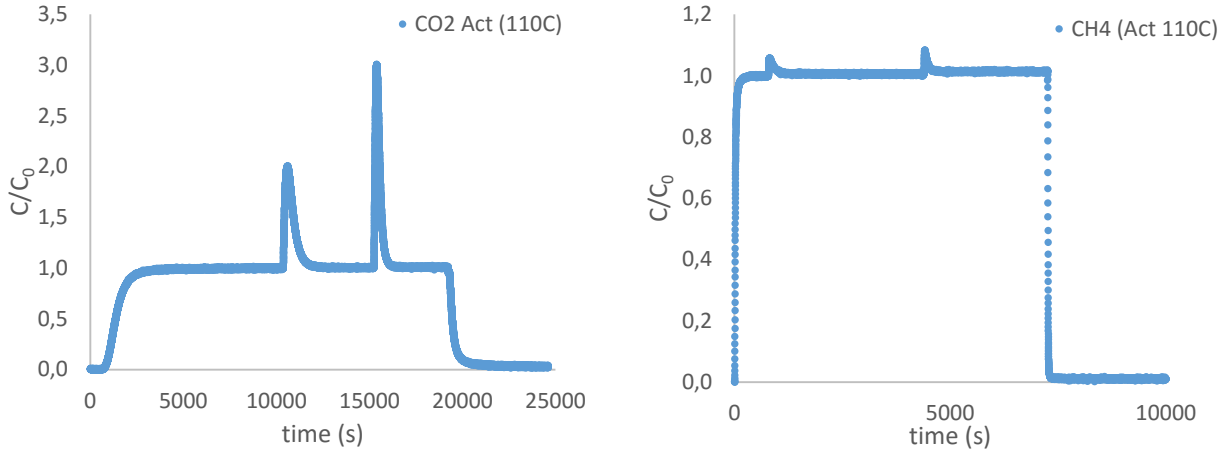

Figure 20 Breakthrough curves obtained using Method B using a UPRM-5 sample activated at 110ºC

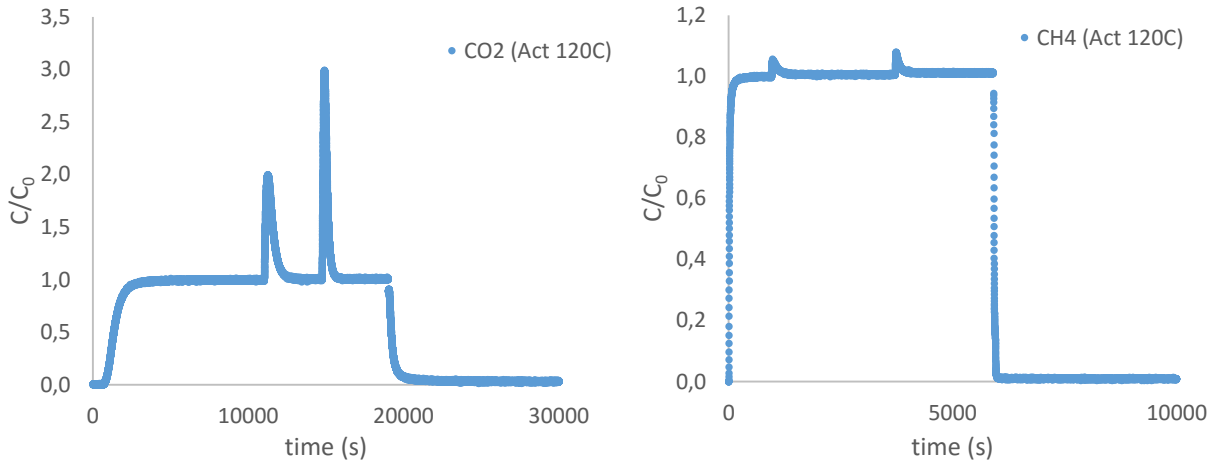

Figure 21 Breakthrough curves obtained using Method B using a UPRM-5 sample activated at 110C

As it was seen before, CH_4 breaks through the column extremely fast and CO_2 takes longer to breakthrough.

The stoichiometric time at 26ºC was calculated as in the method A. The stoichiometric times for 40ºC and 70ºC were estimated subtracting the area below each peak to this stoichiometric time.

$$(t_{st})_{40°C} = (t_{st})_{26°C} - Area_{peak01} \quad (29)$$

$$(t_{st})_{70°C} = (t_{st})_{40°C} - Area_{peak02} \quad (30)$$

The parameters calculated for each method, such as stoichiometric time, Henry's constant, and isosteric heat of adsorption, are presented in tables 4 and 5 for CO2 and CH4 respectively.

Table 4 Stoichiometric time, Henry's constant and isosteric heat of adsorption for the breakthrough curves of CO2 at different activation temperatures

		Method A			Method B		
Activation temperature (ºC)	**Measurement temperature (ºC)**	**t_{st} (s)**	**H ($cm^3.g^{-1}$)**	**-ΔH ($kJ.mol^{-1}$)**	**t_{st} (s)**	**H ($cm^3.g^{-1}$)**	**-ΔH ($kJ.mol^{-1}$)**
80	26	1028	517	22.1	1082	544	28.8
	40	668	336		664	334	
	70	328	164		247	124	
90	26	1198	602	26.9	1173	590	30.3
	40	662	333		710	357	
	70	295	148		249	125	
100	26	1434	721	20.7	1456	732	27.1
	40	801	403		914	460	
	70	476	239		362	181	
110	26	1677	843	29.1	1507	758	28.3
	40	935	470		945	475	
	70	371	186		354	177	
120	26	1625	817	28.9	1482	745	28.4
	40	902	453		932	469	
	70	362	182		346	174	

With both methods higher adsorbed CO_2 amounts were attained when the sample was pre-treated at 110ºC, although the difference with other activation temperatures is very small.

The breakthrough experiments obtained with sample activated at this temperature, should be repeated, since these results are not coherent with the ones obtained with the adsorption equilibrium isotherms.

Table 5 Stoichiometric time, Henry's constant and isosteric heat of adsorption for the breakthrough curves of CH_4 at different activation temperatures

		Method A			Method B		
Activation temperature (ºC)	**Measurement temperature (ºC)**	**t_{st} (s)**	**H ($cm^3.g^{-1}$)**	**-ΔH ($kJ.mol^{-1}$)**	**t_{st} (s)**	**H ($cm^3.g^{-1}$)**	**-ΔH ($kJ.mol^{-1}$)**
80	26	21	13.31	15.3	20	9.30	11.1
	40	14	8.53		15	7.01	
	70	10	5.85		12	5.17	
90	26	20	13.17	12.0	26	12.49	10.1
	40	16	10.42		21	9.78	
	70	12	7.06		16	7.32	
100	26	27	17.53	15.3	26	12.4	11.2
	40	20	12.99		20	9.55	
	70	13	7.93		15	6.89	
110	26	22	14.12	13.3	25	12.1	12.2
	40	20	12.61		19	9.13	
	70	12	7.28		14	6.39	
120	26	26	16.94	15.9	25	12.0	11.6
	40	20	12.52		20	9.26	
	70	12	7.43		14	6.56	

The values obtained through both methods are not so far apart that can be considered wrong, but some breakthrough experiments should be repeated to validate some results. Even though some were repeated, the CO_2 desorption takes quite some time under the measurement conditions, limiting the amount of repetitions.

Some breakthrough experiments results could have been slightly affected by the valve malfunctioning, since it had to be adjusted several times. In other hand, stoichiometric time is so small, in most cases, that minimal chronometer reading delays could be greatly amplified. This can justify the small differences in the stoichiometric times calculated over both methods.

6 Conclusions

Sr2+UPRM5 was studied to separate kinetically carbon dioxide and methane.

XRD data concluded that the higher structure contraction took place between 70ºC and 100ºC. With this in mind 80, 90, 100, 110 and 120 ºC were the chosen activation temperatures.

Adsorption Isotherms of the pure components carbon dioxide and methane were measured at 25ºC and successfully fitted to the Sips model. The adsorbent showed higher affinity towards CO_2 and higher adsorbed amount was attained when the sample was pre-treated at 110ºC. However the sample pre-treated at 110ºC didn't reach the highest adsorbed amounts in the complete pressure range studied. The gaseous concentration should always be in mind when the temperature activation is being chosen.

Breakthrough experiments were performed using two different methods, the traditional breakthrough curves and temperature programmed desorption breakthrough curves, validating the kinetic separation of the gaseous mixture using Sr^{2+}UPRM5. Even though some test should be repeated.

A mathematical model was used to simulate the breakthrough curves using the gPROMS software. The simulation results were not as expected, and most should be repeated in order to obtain diffusion rates.

6.1 Future work

Breakthrough experiments should be performed with a CO_2/CH_4 mixture, in order to have a more realistic idea of the results that could be expected in the further implementation of Sr^{2+}UPRM-5 adsorbent in a PSA unit.

Throughout the work involved in the last five months, some limitations and challenges were faced in both the experimental and modelling phases. Some of which were not possible to overcome due to the time restrictions of the project, or instruments malfunctioning.

During the GC operation, the six-positions-valve had to be adjusted several times. This setback prolonged the time spent during the breakthrough experiments. This might have influenced some of the breakthrough experiments, repetition of some breakthrough tests could only be beneficial to reassure the results.

A more complex mathematical model could be developed to simulate the Temperature Programmed Desorption Breakthrough Curves. The model fitting to the breakthrough data could be improved, with more time. All the other breakthrough curves should also be simulated,

however this was not possible due to technical issues related with the gPROMS programs functionality, combined with lack of time.

7 Bibliography

[1] – KASMAN, A., Duman, Y.S. (2014) – CO2 emissions, economic growth, energy consumption trade and urbanization in new EU member and candidate countries: A panel data analysis. Elsevier: Economic Modelling (44), 97-103. [consulted in 20 Aug. 2015]. Available in www.<URL: http://dx.doi,org/10.1016/j.econmod.2014.10.022>

[2] – Crespo, P. S. Aminoterephthalate Metal-Organic Frameworks: Syntesis, Characterization and Applications. (2014). The Netherlands: Delft University of Technology.

[3] – LI, Jian-Rong; MA, Yuguang; McCARTHY, M. Colin; SCHULLEY, Julian; YU, Jiamei; JEONG, Hae-Kwon; BALBUENA, Perla B.; ZHOU, Hong-Cai. (2011) – Carbon dioxide capture-related gas adsorption and separation in metal-organic frameworks. Elsevier: Coordination Chemistry Reviews, 255, 1791-1823. [consulted in 24 Aug. 2015]. Available in www.<URL: http://dx.doi.org/10.1016/j.ccr.2011.02.012>

[4] - International Energy Agency (2014). Key World Energy Statistics

[5] – Environment.no, Norway's Climate http://www.environment.no/topics/climate/norways-climate/#D [consulted in 08 Sept. 2015]

[6] – Environment.no, Impacts of climate change in Norway http://www.environment.no/Topics/Climate/Norways-climate/Impacts-in-Norway/ [consulted in 08 Sept.2015]

[7] – Environment.no, Driving forces in Norway http://www.environment.no/Topics/Climate/Norways-climate/Driving-forces-in-Norway [consulted in 08 Sept.2015]

[8] – PRIMERA-PEDROZO, J. N.; TORRES-COSME, B.D.;CLARDY, M. E.; RIVERA-RAMOS, M. E.; HERNÁNDEZ-MALDONADO, A. J. (2010) – Titanium Silicate Porous Materials for Carbon Dioxide Adsorption: Synthesis Using a Structure Directing Agent, Detemplation and Inclusion of Alkaline Earth Metal Cations. Industrial & Engineering Chemistry Research, 49, 7515-7523. [consulted. in 12 Aug. 2015]. Avaible in www.<URL: http://dx.doi.org/10.1021/ie100331q>

[9] – U.S. Energy Information Administration (2013) Carbon Dioxide Emissions Coefficients [consulted in 01 Sept. 2015]. Available in http://www.eia.gov/environment/emissions/co2_vol_mass.cfm

[10] – XIAO, Youchang; LOW, Bee Ting; HOSSEINI, Seyed Saeid; CHUNG, Tai Shung; PAUL, Donald Ross. (2009) – The startegies of molecular architecture and mofification of polyimide-based membranes for CO_2 removal from natural gas – A review. Elsevier: Progress in Polymer Science,

34, 561-580. [Consulted in 24 Aug. 2015]. Available in www.<URL: http://dx.doi.org/10.1016/j.progpolymsci.2008.12.004>

[11] – LARA-GARCÍA, Hugo A.; GONZALEZ, Maximiliano R.; GONZÁLEZ-ESTEFAN, Juan H.; SÁNCHEZ-CAMACHO, Pedro; LIMA, Pedro; IBARRA, Ilich A. (2015) – Removal of CO2 from CH4 and CO2 capture in the presence of H2O vapour in NOTT-401. Inorganic Chemistry Frontiers, 2, 442. [Consulted in 19 Aug. 2015]. Available in www.<URL: http://dx.doi.org/10.1039/c5qi00049a>

[12] – CAVENATI, Simone; GRANDE, Carlos A.; RODRIGUES, Alírio E. (2004) – Adsorption Equilibrium of Methane, Carbon Dioxide, and Nitrogen on Zeolite 13X at High Pressures. Journal of Chemical Engineering Data, 49, 1095-1101. [Consulted in 20 Aug. 2015]. Available in www.<URL: http://dx.doi.org/10.1021/je0498917>

[13] – YU, Moxin; PRIMERA-PEDROZO, José; MARCANO-GONZÁLEZ, Marietta; HERNÁNDEZ-MALDONADO, Arturo J. (2014) – Selective adsorption of N_2 over CH_4 in flexible Sr^{2+} - and Ba^{2+}-UPRM-5 (TEA) titanium silicates: Effect of activation temperature. Elsevier: Chemical Engineering Journal, 252, 311-319. [Consulted in 12 Aug. 2015]. Available in www.<URL: http://dx.doi.org/10.1016/j.ces.2014.

05.034>

[14] - Marcano-González, M. E.; Fu, R.; Hernández-Maldonado, A. J. (2015) - Long- and Local-Range Structural Changes in Flexible Titanium Silicates with Variable Faulting upon Thermal Treatment and Corresponding Adsorption and Particle Size Polydispersity-Corrected Diffusion Parameters for CO_2/CH_4 Separation. Industrial & Engineering Chemistry Research, 54, 207-216.[consulted. in 12 Aug. 2015]. Available in www.<URL: http://dx.doi.org/10.1021/ ie5046044>

[15]- BAKER, Richard W.; LOKHANDWALA, Kaaeid (2008) – Natural Gas Processing with Membranes: Na Overview. Industrial & Engineering Chemistry Research, 47 (7), 2109-2121. [consulted in 20 Aug. 2015]. Available in www.<URL: http://dx.doi.org/10.1021/ie071083wtt>

[16]- CAVENATI, Simone; GRANDE, Carlos A.; RODRIGUES, Alírio E. (2006) – Removal of Carbon Dioxide from Natural Gas by Vacuum Pressure Swing Adsorption. Energy & Fuels, 20, 2648-2659. [consulted in 19 Aug. 2015]. Available in www.<URL: http://dx.doi.org/10.1021/ ef060119e >

[17] – TAGLIABUE, Marco; FARRUSSENG, David; VALENCIA, Susana; AGUADO, Sonia; RAVON, Ugo; RIZZO, Caterina; CORMA, Avelino; MIRODATOS, Claude. (2009) – Review: Natural gas treating by selective adsorption: Material science and chemical engineering interplay. Elsevier: Chemical Engineering Journal, 155, 553-566. [consulted in 24 Aug. 2015]. Available in www.<URL: http://dx.doi.org/10.1016/j.cej.2009.09.010>

[18]- Marcano-González, M. E.; Primavera-Pedrozo, J. N.; Jiménez-Laureano, Z.; Fu, R.; Hernández-Maldonado, A. J. (2013)- UPRM-5 titanium silicates prepared using tetrapropylammonium and tetrabutylammonium cations: framework stability, textural properties, and carbon dioxide adsorption. J Mater Sci, 48, 2053-2066. [consulted. in 12 Aug. 2015]. Avaible in www.<URL: http://dx.doi.org/10.1007/s10853-012-699978-x>

[19] – CAVENATI, Simone; GRANDE, Carlos, A.; RODRIGUES, Alírio E. (2006) – Separation of CH_4/ CO_2/N_2 mixtures by layered pressure swing adsorption for upgrande of natural gas. Elsevier: Chemical Engineering Science, 61, 3893-3906. [consulted in 19 Aug. 2015]. Available in www.<URL: http://dx.doi.org/10.1016/j.ces.2006.01.023>

[20] – DELGADO, José A.; UGUINA, María A.; GÓMEZ, José M.; ORTEGA, Luís. (2006) – Adsorption equilibrium of carbon dioxide, methane and nitrogen onto Na- and H-mordenite at high pressures. Elsevier: Separation and Purification Technology, 48, 223-228. [consulted in 24 Aug. 2015]. Available in www.<URL: http://dx.doi.org/10.1016/j.seppur.2005.07.027>

[21] – BASTIN, Laurent; BÁRCIA, Patrick S.; HURTADO, Eric J.; SILVA, José A. C.; RODRIGUES, Alírio E.; CHEN, Banglin. (2008) – A Microporous Metal – Organic Framework for Separation of CO_2/N_2 and CO_2/CH_4 by Fixed-Bed Adsorption. The Journal of Physical Chemistry C, 112, 1575-1581. [consulted in 19 Aug. 2015]. Available in www.<URL: http://dx.doi.org /10.1021/jp077618g>

[22] - CAVENATI, Simone; GRANDE, Carlos A.; Rodrigues, Alírio E. (2006) Removal of Carbon Dioxide from natural gas by vacum pressure swing adsorption. Energy & Fuels, 20, 2648-2659. [consulted in 13 Sept. 2015]. Avaible in www.<URL: http://dx.doi.org/10.1021/ef060119e >

[23] - Geochemical Instrumentation and Analysis: X-ray Powder Diffraction (XRD) http://serc.carleton.edu/research_education/geochemsheets/techniques/XRD.html [consulted in 11 Sept. 2015]]

[24] – RUTHVEN,D. M. Principles of Adsorption and Adsorption Processes, Wiley: New York, 1984.

[25] - SIPS, R. (1948) On the structure of a catalyst surface, J. Chem. Phys., 16, 490-495

[26] – GRANDE, Carlos A. (2004) Propane / Propylene separation by adsorption processes, Faculty of Engineering – University of Porto.